Journal of Nuclear Materials xxx (2013) xxx–xxx

Contents lists available at SciVerse ScienceDirect

Journal of Nuclear Materials

journal homepage: www.elsevier.com/locate/jnucmat

Plasma facing surface composition during NSTX Li experiments

C.H. Skinner [a,*,1], R. Sullenberger [b], B.E. Koel [c], M.A. Jaworski [a], H.W. Kugel [a]

[a] Princeton Plasma Physics Laboratory, POB 451, Princeton, NJ 08543, USA
[b] Department of Mechanical and Aerospace Engineering, Princeton University, NJ 08540, USA
[c] Department of Chemical and Biological Engineering, Princeton University, NJ 08540, USA

ARTICLE INFO

Article history:
Available online xxxx

ABSTRACT

Lithium conditioned plasma facing surfaces have lowered recycling and enhanced plasma performance on many fusion devices. However, the nature of the plasma–lithium surface interaction has been obscured by the difficulty of in-tokamak surface analysis. We report laboratory studies of the chemical composition of lithium surfaces exposed to typical residual gases found in tokamaks. Solid lithium and a molybdenum alloy (TZM) coated with lithium have been examined using X-ray photoelectron spectroscopy, temperature programmed desorption, and Auger electron spectroscopy both in ultrahigh vacuum conditions and after exposure to trace gases. Lithium surfaces near room temperature were oxidized after exposure to 1–2 Langmuirs of oxygen or water vapor. The oxidation rate by carbon monoxide was four times less. Lithiated PFC surfaces in tokamaks will be oxidized in about 100 s depending on the tokamak vacuum conditions.

1. Introduction

Liquid plasma facing materials avoid serious issues with radiation damage, helium blisters, thermal fatigue and erosion lifetime in solids. Though less developed than solid plasma facing components, they enable the separation of the demands from neutron loading and the demands from heat and particle loading placed on plasma facing components in a fusion reactor. Liquid lithium has the further advantage of binding with hydrogen isotopes, and lithium conditioning has reduced recycling and enhanced plasma performance on many fusion devices.

Lithiumization of carbon plasma-facing components led to substantial advances in plasma performance in TFTR [1]. These were followed by experiments with a liquid Li capillary pore system at T11-M [2] and FTU [3], with a liquid Li tray in CDX-U [4] and with lithiumization of the TJ-II stellerator [5]. A new liquid Li tokamak (LTX) began operation in 2010 [6]. Lithiumization of ATJ graphite plasma facing tiles in the National Spherical Torus Experiment (NSTX) has shown strong beneficial effects such as improved confinement and reduction and elimination of ELMs [7,8]. 2-D plasma-neutrals modeling has shown a drop in divertor recycling from $R \sim 0.98$ to $R \sim 0.9$ with lithium [9]. A recent overview of lithium applications for fusion devices is given in Ref. [10].

To understand the plasma–lithium surface interaction and provide a design basis for next-step plasma facing components that take advantage of the benefits of lithium, it is important to characterize the chemical composition of the plasma facing lithium surface. Lithium is known to have a high chemical affinity for hydrogen and full uptake of deuterium ions on a liquid Li surface up to an atomic ratio of 1:1 was reported in the PISCES-B linear plasma simulator [11]. We note that the NSTX recycling reduction from $R \sim 0.98$ to $R \sim 0.9$ [9] falls short of complete uptake suggesting surface chemistry is playing a role in NSTX. In the PISCES work, 0.1 g of Li was press fit into a molybdenum holder and surface contamination was removed by high-flux plasma exposure with the Li in its liquid state. However, X-ray photoelectron spectroscopy (XPS) measurements indicated that at least monolayer coverage of Li_2O was still present after this cleaning. Early work on lithium battery development exposed lithium films to gaseous O_2, H_2O, CO, CO_2, and SO_2 [12,13]. XPS measurements on Li films at 300 K showed monolayer Li_2O coverage occurred for oxygen exposures between 6 and 7 Langmuirs (L) and water vapor exposures of 11–12 L (1 Langmuir (L) is defined as an exposure of 1e−6 Torr (1.33e−4 Pa) for 1 s). An additional complication for liquid Li surfaces was revealed by low energy ion scattering experiments [14] that showed the Gibbsian segregation of oxygen impurities to the surface of liquid lithium. XPS spectra of Li deposited on ATJ graphite have been interpreted to indicate peroxide formation due to oxygen impurities in the chamber [15]. The special role of oxygen in deuterium uptake on lithiated graphite is further explored in Ref. [16]. Deuterium ion–surface interactions [17] and high sputtering rates [18] of liquid-Li films on microporous molybdenum substrates have been reported.

Since tokamaks typically do not have ultrahigh vacuum (UHV) conditions, surface reactions with residual gases may occur in the time interval between lithium evaporation and the next

* Corresponding author. Tel.: +1 609 243 2214; fax: +1 609 243 2665.
E-mail address: cskinner@pppl.gov (C.H. Skinner).
[1] Presenting author.

0022-3115/$ - see front matter © 2013 Elsevier B.V. All rights reserved.
http://dx.doi.org/10.1016/j.jnucmat.2013.01.136

discharge. Recently surface analysis stations have been developed for ex vessel but in vacuo surface analysis of samples withdrawn after tokamak exposure [19,20]. However, much of the relevant surface chemistry is accessible in laboratory investigations using sophisticated surface analysis instruments that are difficult to implement inside a tokamak vacuum vessel.

We report high-resolution X-ray photoelectron spectroscopy (HR-XPS), Auger electron spectroscopy (AES), and temperature programmed desorption (TPD) investigations of the oxidation of lithium surfaces by gases typically found in a tokamak residual vacuum such as water and carbon monoxide as well as oxygen and air and compare the oxidation rate to the kinetics of gases impinging on the surface. A more extensive account of this work is in Ref. [21].

2. High resolution X-ray photoelectron spectroscopy

High-resolution XPS (HR-XPS) measurements were performed with a Scienta ESCA-300 system [22] with a 7.5 kW rotating anode monochromatic Al Kα X-ray source. A small (<5 g) piece of lithium was cut from 99.9% purity lithium rod [23] and compressed between two aluminum plates to create a sample approximately 10-mm diameter and 1-mm thick. This was transferred into a nitrogen-filled glove bag attached to the ESCA-300 sample preparation chamber and a metal scraper was used to clean the surface. After sufficient scraping, the appearance of the lithium changed from white to shiny, indicating most of the oxide had been removed. The sample was then promptly loaded into the ESCA-300.

The lithium sample holder was allowed to degas for a day until UHV conditions were recovered (3e−9 Torr; 4.0e−7 Pa) and then a tungsten carbide-tipped scraper was used to further clean the lithium surface while monitoring the XPS spectrum. An XPS survey scan (0–800 eV) of a typical freshly-scraped lithium surface revealed O 1s (532 eV binding energy (BE)) and Li 1s (54.8 eV BE) photoelectron peaks with a small peak due to C 1s (285 eV BE). The scraping was repeated after each oxidation experiment and the surface was considered clean when analysis using CasaXPS software [24] showed an atomic concentration of >95% lithium (the remainder on average was 4% O and 1% C). For each oxidation experiment the chamber was backfilled with oxygen (O_2), air, water vapor (H_2O) or carbon monoxide (CO) to ~7.0e−8 Torr (9.3e−6 Pa) and the sample was exposed to the gas for a variable time interval (15–9500 s) after which the chamber was pumped out and XPS spectra recorded in the Li 1s, O 1s and C 1s energy regions. The sample temperature was ~300 K for all experiments. The gas exposure process was continued until the 54.8 eV metallic lithium peak was less than 10% of its original area. The XPS spectra for increasing H_2O exposures are shown in Fig. 1. The increase in the oxide concentration was calculated from the area under the Li–O 56.6 eV XPS peak for all gases and is shown in Fig. 2. XPS is considered to sample the surface composition down to a depth of three times the inelastic mean free path (imfp, λ) for electron scattering at the kinetic energy (KE) of the photoelectron line used. The value of λ for Li 1s photoelectrons (1431 eV KE) in Li_2O is 3.47 nm [25]. We observed that the lithium surface was oxidized to this depth after 20 L exposure to water vapor or oxygen. Carbon monoxide and air were about six times less reactive.

The fraction of the bulk lithium oxide Li 1s photoelectron signal that can be attributed to the top monolayer (ML) at the surface of lithium oxide can be calculated to be 6.6% by using the ratio of the thickness of a Li_2O monolayer, 0.231 nm, to the value of λ, 3.47 nm, for Li 1s photoelectrons at (1431 eV KE) in Li_2O using the formula of Argile [26]. Including a small contribution from residual gas exposure during the pressure ramp-up and XPS scans, the water vapor exposure for oxidation of the top monolayer was estimated

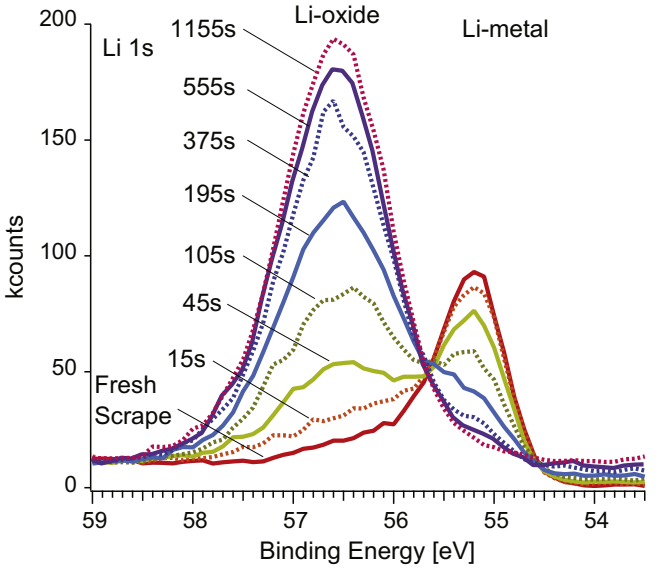

Fig. 1. HR-XPS spectra in the Li 1s region showing the transformation of lithium to lithium-oxide after exposure to water vapor at 6.2e−8 Torr.

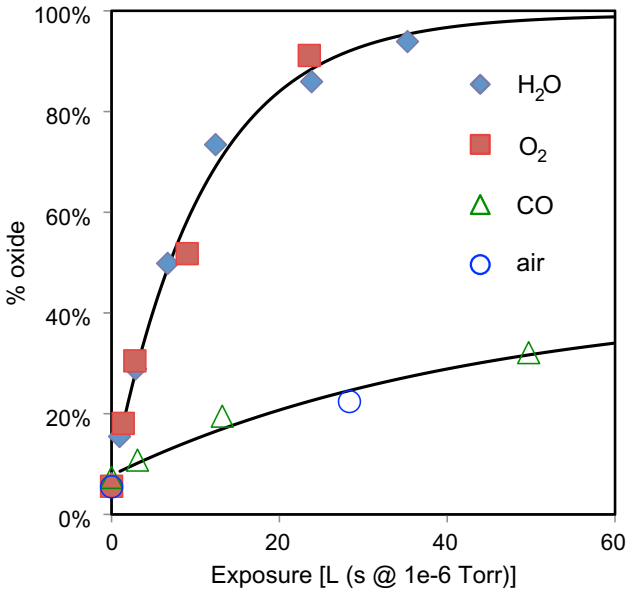

Fig. 2. Oxidation uptake plots using the area of the Li-oxide 56.6 eV BE HR-XPS peak to follow the growth of Li-oxide with increasing exposure to several gases. Exposures were corrected for ion gauge sensitivity. The lines are a visual aid.

to be 1.3 L. This is similar to the value of 1.35 L calculated from kinetic theory [27] for a smooth lithium surface oxidized to Li_2O by impinging water molecules with unity sticking coefficient.

3. Auger electron spectroscopy

Auger electron spectroscopy (AES) measurements were performed with a versatile UHV system containing several complementary surface analysis probes [28]. In AES, core electrons are ejected by an incident electron beam and the core hole is filled by a two-electron non-radiative relaxation process (Auger process) in which an (Auger) electron is ejected with the kinetic energy required to conserve energy. For Auger processes involving core holes, Auger kinetic energies uniquely identify the atom and the

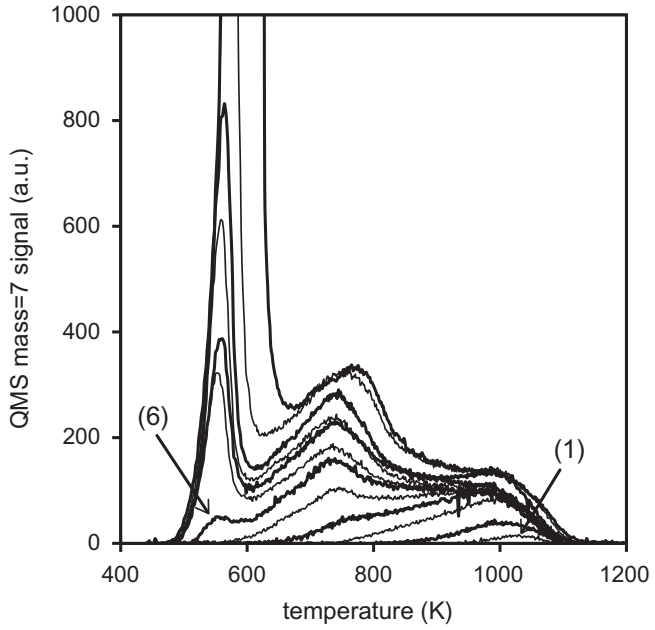

Fig. 3. TPD spectra of lithium (7 amu) desorption from films of increasing amount on a TZM substrate. TPD peak (1) at 1040 K is characteristic of strong Li–TZM interactions. The TPD trace (labeled 6) first showed a peak at 560 K that is attributed to multilayer lithium desorption.

analysis of Auger electrons at energies below 1 keV provides surface sensitivity. The Auger electron spectrum typically has small peaks on a large background and so the signal is differentiated to make it easier to analyze.

Lithium coatings on a polycrystalline TZM substrate (TZM is an alloy composed of 99% Mo, 0.5% Ti and 0.08% Zr) were used for these AES studies since this material is being considered for NSTX-U. The sample was prepared initially by polishing with silicon carbide paper (800 grit) followed by an acetone wipe. Gross surface contamination was removed in the analysis chamber by Ar^+ ion sputtering and resistively heating the sample to 1650 K. This removed all the oxygen and reduced the amount of carbon signal to 30 at%, the balance being 65 at% Mo and 5 at% Ti. Oxygen treatments could remove all of the carbon, but upon heating to remove oxygen, carbon always reappeared, and so we utilized the carbon-contaminated surface for these experiments. Some carbon contamination is considered tokamak relevant, as carbon is a common impurity in tokamaks.

A SAES Getters alkali metal dispenser (AMD) [29] was used to deposit a controlled amount of pure lithium onto the TZM surface. The AMD was powered for 1 min with a fixed current to reach a steady evaporation rate, then the TZM sample was lowered to be 1 cm in front of the AMD for a set time interval, after which the electrical current was switched off. The amount of deposited lithium was calibrated by temperature programmed desorption (TPD) using a 10 K/s linear temperature ramp up to 1200 K. Lithium (7 amu) desorption was tracked during heating with a quadrupole mass spectrometer with the ionizer in direct line-of-sight with the sample and is shown in Fig. 3. After each TPD scan, an increasing dose of lithium was reapplied by increasing the dosing time at a constant Li flux. The smallest lithium dose, at a current of 5.04 A for 30 s, produced a TPD peak at 1040 K characteristic of strong Li–TZM interactions (curve 1 in Fig. 3). A second peak appeared at 750 K with increasing Li dose. When the Li dispenser was operated at 5.04 A for 180 s, a third peak appeared near 560 K (curve 6 in Fig. 3). This peak corresponds to a desorption activation energy of 1.5 eV, close to the cohesive energy (1.69 eV) of metallic lithium [30] and is attributed to desorption from a lithium multilayer. The threshold lithium dose resulting in the appearance of this peak is defined as that required for producing a single monolayer of lithium. Using this value we calculate that the Li flux in these experiments was 0.0056 ML/s. A similar TPD pattern was found for lithium desorbing from a Ni(1 1 0) surface [31].

AES was performed with a PHI 15-225G cylindrical mirror electron analyzer (CMA) with a 3 kV, 5.2 μA incident electron beam in a UHV chamber [28] with a base pressure of 5e−10 Torr (6.7e−8 Pa). We utilized control software to do time-resolved AES measurements in which a new AES spectrum was acquired every 3.6 s during the oxidation process. A lithium film was deposited on a TZM substrate at 350 K by operating the AMD at 5.18 A for 300 s. This produced a TPD curve with 6.8 times the area of a TPD curve with the 560 K peak (curve (6) in Fig. 3) and hence corresponds to a lithium deposition of 6.8 monolayers. An initial AES scan verified that the surface oxygen concentration was less than 2% and then the chamber was backfilled to 1e−8 Torr (1.33e−6 Pa) with O_2, CO, or H_2O. The oxygen uptake was measured dynamically by repeated AES scans every 3.6 s over the O(KVV) region (480–530 eV) up to an exposure of 12 L. A control experiment was performed to verify that there was no influence by the incident electron beam. Fig. 4 illustrates the results for oxygen exposure.

The experiment was repeated for water vapor and carbon monoxide and the combined results are shown in Fig. 5. It can be seen that saturation in the O(KVV) signal occurred near 5 L for O_2 and H_2O. The AES probing depth is given by three times the *imfp* (λ), where λ is 1.62 nm for the 513 eV KE O(KVV) electron [25], times the cosine of the electron take-off angle of 42.5° (in these experiments). This depth is 3.6 nm, so AES probes the complete 1.6 nm thickness of the Li_2O film assuming a uniform coating. The metallic Li(KVV) AES peak disappeared during the gas exposures used showing that the whole film is oxidized. From the data in Fig. 5 we calculate that oxidation to produce one monolayer of Li_2O occurs after an exposure of ~1 L of H_2O or O_2, which is a result similar to that from the XPS data for a solid Li sample. This value

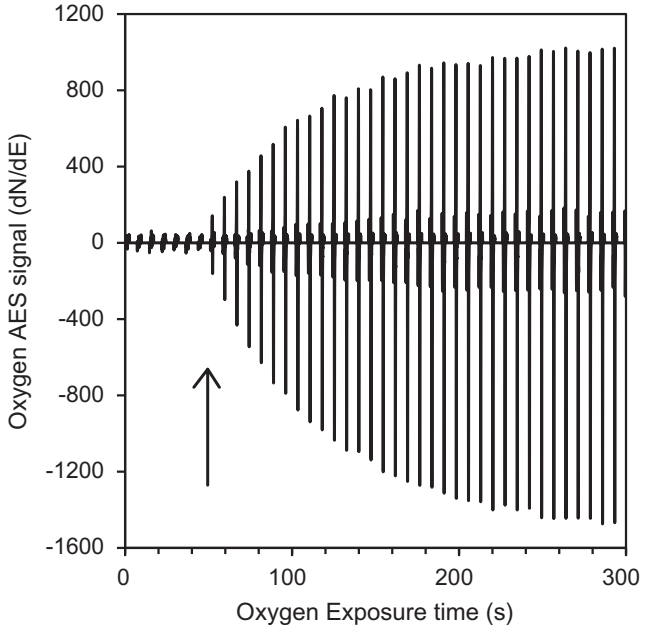

Fig. 4. Oxidation uptake plot showing repeated scans over the O(KVV) AES energy region (480–530 eV KE) for TZM coated with a 6.8 ML Li film during exposure to oxygen starting at the time denoted by the arrow. The oxygen near surface concentration is proportional to the peak-to-peak height of the differentiated AES signal.

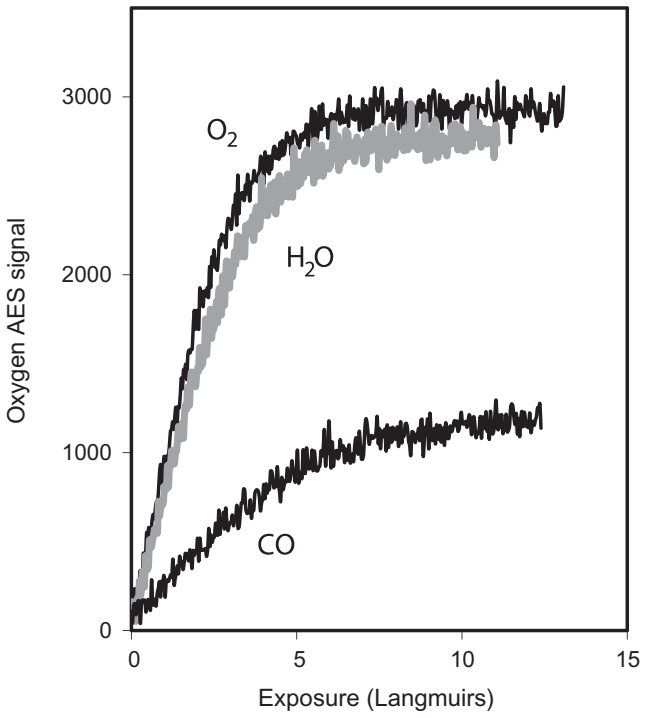

Fig. 5. Oxidation uptake plots for a 6.8 ML lithium film on TZM obtained using the procedure depicted in Fig. 4. Plots are for exposure to O_2 (top curve), water vapor (middle grey curve) and carbon monoxide (bottom curve).

is significantly lower than the 11–12 L reported for H_2O in Ref. [13] but our reanalysis of that data gives a result consistent with our measurement. As shown in Fig. 5 the O (KVV) AES signal rise for CO was four times slower than for H_2O, which is also consistent with the XPS results that indicated ~six times slower oxidation from CO compared to H_2O.

4. Discussion and conclusions

The chemical composition of a plasma facing lithium surface is a key factor in lithium's capability to absorb hydrogen isotopes and plasma impurities. The NSTX base vacuum is typically in the low 1e−8 Torr (1.3e−6 Pa) range. However immediately after a discharge it rises to 3e−6 Torr (4e−4 Pa) and is pumped out by a combination of turbomolecular pumps and cryopumps in the neutral beam box to a pressure below 1e−7 Torr (1.3e−5 Pa) before the next discharge. Residual gas analysis shows the main constituents of the gas are hydrogenic species (77% mass 2, 3, 4) and water vapor (18% mass 17, 18, 19, 20). The intershot interval is 600 s or longer and lithium evaporation occurs during this time. Depending on the timing of the opening of the neutral beam valve, the vessel walls are exposed to 100–600 L of water vapor.

Our HR-XPS and AES results above show that the top monolayer of a lithium film is oxidized by 1–2 L of water vapor or oxygen. The oxidation rate for carbon monoxide is about four times slower. TRIM calculations [32] show the stopping range of ~100 eV deuterium ions in lithium or lithium oxide is ~5 nm or ~20 monolayers of Li_2O and is similar to the range probed by XPS and AES. The results indicate that the NSTX PFC surface layer that is accessible by plasma deuterium ions will be oxidized after 20–40 L exposure to water vapor in the NSTX residual vacuum and the PFC surface at the initiation of the discharge should be considered as a mixed material rather than a pure 'lithium coating'. Oxygen can also combine with and trap deuterium, and a complex carbon–lithium–oxygen–deuterium chemistry is reported in Ref. [16]. Follow-up studies using scanning Auger microscopy on other lithium coated substrates, including single crystal molybdenum are planned.

Acknowledgements

The authors thank E. Kearns and X. Yang for technical assistance. The HR-XPS experiments were performed in the Scienta ESCA-300 facility at LeHigh University with technical assistance by Dr. A. Miller. Support is provided by the US DOE Contract No. DE AC02-09CH11466.

References

[1] D.K. Mansfield et al., Phys. Plasmas 3 (1996) 1892.
[2] S.V. Mirnov et al., Plasma Phys. Controlled Fusion 48 (2006) 821.
[3] M.L. Apicella et al., J. Nucl. Mater. 386–388 (2009) 821.
[4] R. Kaita et al., Phys. Plasmas 14 (2007) 056111.
[5] J. Sanchez et al., Nucl. Fusion 49 (2009) 104018.
[6] R. Kaita et al., Fusion Eng. Des. 85 (2010) 874.
[7] H.W. Kugel et al., J. Nucl. Mater. 390–391 (2009) 1000.
[8] M.G. Bell et al., Plasma Phys. Controlled Fusion 51 (2009) 124054.
[9] J.M. Canik et al., J. Nucl. Mater. 415 (2011) S409.
[10] M. Ono et al., Nucl. Fusion 52 (2012) 037001.
[11] M.J. Baldwin et al., Nucl. Fusion 42 (2002) 1318.
[12] J.R. Hoenigmann, R.G. Keil, App. Surf. Sci. 18 (1984) 207.
[13] J.R. Hoenigmann, R.G. Keil, in: R.O. Bach (Ed.), Lithium Current Applications in Science, Medicine and Technology, Wiley, New York, 1985, p. 243.
[14] R. Bastasz, J.A. Whaley, Fusion Eng. Des. 72 (2004) 111.
[15] S.S. Harilal et al., Appl. Surf. Sci. 255 (2009) 8539.
[16] P. Krstic et al., Phys. Rev. Lett. (2013), in press.
[17] B. Heim et al., Nucl. Instrm. Methods Phys. Res. B 269 (2011) 1262.
[18] M. Nieto-Perez et al., J. Nucl. Mater 415 (2011) S133.
[19] C.H. Skinner et al., J. Nucl. Mater. 415 (2011) (2011) S773.
[20] B. Heim et al., IEEE Trans. Plasma Sci. 40 (2012) 735.
[21] R. M. Sullenberger (2012), Uptake and Retention of Residual Vacuum Gases in Lithium and Lithium Films, M.Sc. thesis, Princeton University, 2012, unpublished.
[22] G. Beamson et al., Surf. Interface Anal. 15 (1990) 541.
[23] supplied by FMC Lithium, 2801 Yorkmont Road, Charlotte, NC 28208.
[24] http://www.casaxps.com/.
[25] C.J. Powell, A. Jablonski, NIST Electron Inelastic-Mean-Free-Path Database, Version 1.2, SRD 71, NIST, Gaithersburg, MD, 2010.
[26] C. Argile, G. Rhead, Surf. Sci. Rep. 10 (1989) 277.
[27] A. Roth, 'Vacuum Technology', third ed., P. 3 Table 1.2 and P. 36.
[28] A. Sellidj, B.E. Koel, J. Phys. Chem. 97 (1993) 10076.
[29] SAES Getters USA, Inc. 1122 East Cheyenne Mountain Blvd. Colorado Springs, CO 80906, USA. <http://www.saesgetters.com>.
[30] W. Ching, J. Callaway, Phys. Rev. B 9 (1974) 5115.
[31] V. Saltas, C.A. Papageorgopoulos, Surf. Sci. 461 (2000) 219.
[32] J.F. Ziegler, J.M. Manoyan, Instrm. Methods B35 (1989) 215–228.